ACCSCIENCE PUBLISHING
An International Journal of Optimization and Control: Theories & Applications
ISSN: 2146-0957 eISSN: 2146-5703
Vol.15, No.4, pp.594-609 (2025)
https://doi.org/10.36922/IJOCTA025160082
IJOCTA

RESEARCH ARTICLE

Solving parabolic differential equations via Haar wavelets: A focus on integral boundary conditions

Muhammad Nawaz Khan[1], Masood Ahmad[2], Rashid Jan[3,4,5*], Imtiaz Ahmad[6], and Mohamed Mousa[7]

[1]Institute of Engineering Mathematics, University Malaysia Perlis, Arau, Perlis, Malaysia
[2]Department of Basic Sciences, University of Engineering and Technology, Peshawar, Pakistan
[3] Department of Mathematics, Saveetha School of Engineering (SIMATS), Thandalam, Chennai, Tamil Nadu, India
[4]Department of Mathematics, Khazar University, Baku, Azerbaijan
[5]Institute of Energy Infrastructure (IEI), Department of Civil Engineering, College of Engineering, Universiti Tenaga Nasional (UNITEN), Putrajaya Campus, Jalan IKRAM-UNITEN, Kajang, Selangor, Malaysia
[6]Institute of Informatics and Computing in Energy (IICE), Universiti Tenaga Nasional, Kajang, Selangor, Malaysia
[7]Electrical Engineering Department, Future University in Egypt, Cairo, Egypt
mnawaz77@gmail.com, masood.suf@gmail.com, rashid.jan@uniten.edu.my, imtiazkakakhil@gmail.com, mohamed.Mossa@fue.edu.eg

ARTICLE INFO

Article History:
Received: April 17, 2025
Revised: May 31, 2025
Accepted: June 12, 2025
Published Online: July 7, 2025

Keywords:
Haar wavelets collocation method
Integral boundary conditions
Parabolic differential equations
Numerical analysis

AMS Classification 2010:
26A33; 34A08; 35H15; 34K50
47H10; 60H10

ABSTRACT

The article addresses the solution of parabolic differential equations with integral boundary conditions using the Haar wavelet collocation method. This approach employs a linear combination of Haar wavelet functions to estimate the largest derivatives in the governing equation. The integral boundary conditions are incorporated by repeatedly integrating the highest derivative to formulate equations for the unknowns. Haar wavelets are particularly suitable for approximating solutions to differential equations due to their compact support and multiresolution properties. Numerical experiments on various test cases show that the proposed method yields accurate results, especially when the parameters of the integral boundary conditions are negative.

1. Introduction

Integral boundary conditions play a crucial role in numerous mathematical and physical problems, such as heat conduction and fluid mechanics. These conditions incorporate integrals of the solution over the spatial domain, adding complexity to the use of standard techniques.[1] Research has delved into optimal control problems that involve integral boundary conditions in fields, like physics, engineering, and mechanics.[2,3] The heat conduction problem with integral boundary conditions is notably significant due to its non-self-adjoint nature, which poses challenges for thorough investigation.[4]

Certain chemical diffusion and heat conduction processes are modeled by the nonclassical parabolic initial-boundary value problem[5]:

$$\frac{\partial s}{\partial \mathfrak{t}} = \frac{\partial^2 s}{\partial \varkappa^2} + a\frac{\partial s}{\partial \varkappa} + cs + f(\varkappa, \mathfrak{t}),$$
$$(\varkappa, t) \in (0,1) \times (0, T],$$
$$s(\varkappa, 0) = g_1(\varkappa), \quad \varkappa \in (0,1),$$

*Corresponding Author

$$\begin{aligned} &\frac{\partial s(1,\mathfrak{t})}{\partial \varkappa} = g_2(\mathfrak{t}), \quad \mathfrak{t} \in [0,T], \\ &\int_0^b s(\varkappa,\mathfrak{t})d\varkappa = m(\mathfrak{t}), \quad b \in (0,1),\ \mathfrak{t} \in [0,T], \end{aligned} \tag{1}$$

where a, b, and c are constants, and f, g_1, g_2, and m are prescribed functions.

Various physical and chemical processes can be modeled through the problem (1), as demonstrated in.[5–11] For the purpose of self-containment, we briefly describe some examples here. For instance, if s denotes the concentration of a chemical in a diffusion process, then $m(\mathfrak{t})$ represents the total mass of the chemical in the region $0 < \varkappa < b$ at time $\mathfrak{t}$. Similarly, if s represents the temperature in a heat conduction problem, then $m(\mathfrak{t})$ corresponds to the internal energy content of the region $0 < \varkappa < b$ at time $\mathfrak{t}$. In another example, if s describes the distribution of impurities in a plate over the interval $0 < \varkappa < 1$, the problem (1) models a technological process for the external elimination of gas. This process is applied, for example, in refining silicon plates to remove impurities, where $m(\mathfrak{t})$ represents the total mass of impurities in the plate $0 < \varkappa < 1$. A similar problem arises in biochemistry when $b = 1$ and m are constants. In this case, the condition $\int_0^b s(\varkappa,\mathfrak{t})d\varkappa = m(\mathfrak{t})$ reflects the conservation of the protein.

Numerical methods play a critical role in solving complex mathematical models that arise in science and engineering.[12,13] They enable researchers to simulate real-world phenomena with high accuracy.[14,15] In biomedical sciences, numerical techniques are essential for modeling biological systems, analyzing treatment strategies, and predicting disease progression.[16] Moreover, advancements in numerical algorithms continue to enhance computational efficiency,[17] making large-scale simulations feasible in scientific and industrial applications. In view of the applications of partial differential equations (PDEs) with integral boundary conditions, several methods are used for the efficient solution of these problems. For example, a finite difference method for solving second-order non-linear PDEs with two-point boundary conditions is discussed in,[18] while in,[19] the author applied the finite difference approach to novel boundary value problems. This paper introduces a finite difference method for addressing second-order boundary value problems in ordinary differential equations (ODEs) with an interior singularity.

In,[20] the authors used the finite element method to solve parabolic differential equations with integral boundary conditions related to heat transfer, emphasizing accurate results with minimal computational cost. The study highlights the method's capability to effectively handle sharp transitions over time, including boundary layers, shock layers, and wave fronts. Additionally,[21] discusses error estimates for discretization, further reflecting the method's established reliability. The article[22] introduces an operational matrix method utilizing hybrid Legendre Block-Pulse functions to solve PDEs with nonlocal boundary integral conditions. By applying operational matrices and analyzing convergence through theorems and lemmas, the method reduces integro-PDEs to algebraic systems, demonstrating accuracy and effectiveness through numerical examples compared to established methods. In,[23] the authors used two efficient numerical methods to examine the Poisson equation under distinct nonlocal boundary conditions. Additionally,[24] employs meshless method utilizing radial basis function approximations to interpolate field variables across subdomain boundaries. In,[25] the author addressed a specific type of Schr"odinger equation featuring logarithmic nonlinearity. In,[26] the complex nonlinear Lorenz system is analyzed for accurate parameter estimation and effective reconstruction of the system dynamics,[27] the focus was on higher-order finite-volume methods applied to solve elliptic boundary value problems. These methods ensure accurate solutions to PDEs by demonstrating that their bilinear forms are uniformly elliptic, thereby achieving optimal error estimates. The Haar wavelets collocation method (HWCM) has recently gained traction and is extensively applied in various fields such as signal processing, numerical analysis, and engineering. This method employs the Haar function in several approaches, including the wavelet Galerkin technique,[28] meshless wavelet schemes,[29] wavelet collocation-based schemes,[30] Daubechies wavelet procedure[31] and other weak and strong formulations.[32–35]

Many research efforts have employed diverse Haar function-based methods to solve different problems in science and engineering.[36,37] In,[38] wavelet decomposition is used to filter the original data, effectively removing the negative impact of noise, and enhancing the anomaly detection model's performance. Recently, the Haar wavelet approach has been employed as a mathematical technique for handling differential scenarios, particularly effective in solving parabolic PDEs with integral boundary conditions. Haar wavelets, which form an orthonormal basis for square-integrable functions, are utilized directly

in this method. The HWCM approximates the layout of the differential equations by selecting the midpoints of Haar wavelets as collocation points, where the differential equations are evaluated. The piecewise constant nature of Haar wavelets, forming an orthonormal basis for square-integrable functions, allows them to be directly combined to approximate the set of differential equations. The collocation points are chosen at the midpoints of the Haar wavelets where the differential equation is evaluated.

The content of the rest of the paper is organized as follows: in Section 2, the proposed method is discussed briefly. In Section 3, the implementation procedure of the proposed method is given for 1D and 2D problems. In Section 4, the numerical results and discussion are included. Finally, in Section 5, some conclusions of the proposed work are given.

2. Haar wavelets collocation method

The paper[39] presents the Haar wavelet family for $\varkappa \in [0,1)$:

$$\chi_n(\varkappa) = \begin{cases} 1 & \varsigma_1 \le \varkappa < \varsigma_2, \\ -1 & \varsigma_2 \le \varkappa < \varsigma_3, \\ 0 & \text{otherwise}, \end{cases} \qquad n = 2, 3, ..., \tag{2}$$

where

$$\varsigma_1 = \frac{j}{q}, \qquad \varsigma_2 = \frac{(j+0.5)}{q}, \qquad \varsigma_3 = \frac{(j+1)}{q}, \\ j = 0, 1, \ldots, q-1, \quad q = 2^i, \quad i = 0, 1, \ldots, I. \tag{3}$$

In this context, i represents the upper limit and j represents the lower limit. The index of χ_n is $n = q + j + 1$ in Equation (2). $n = 2q = 2^{I+1}$ is the maximum value of n, where I is the highest resolution level. For $q = 1$ and $j = 0$, the smallest value of n is $n = 2$. The scaling function presumably corresponds to $n = 1$ as follows:

$$\chi_1(\varkappa) = \begin{cases} 1 & 0 \le \varkappa < 1, \\ 0 & \text{otherwise}. \end{cases} \tag{4}$$

In order to solve the PDE problems Equations (32)-Equations (37), we must evaluate the following integrals using Haar wavelets.

$$\Re_{n,1}(\varkappa) = \int_0^{\varkappa} \chi_n(\mathfrak{t})\, d\mathfrak{t}, \tag{5}$$

$$\Re_{n,v}(\varkappa) = \int_0^{\varkappa} \Re_{n,v-1}(\mathfrak{t})\, d\mathfrak{t}, \qquad v = 2, 3, \cdots. \tag{6}$$

An analytical approach for computing these integrals is provided by Equation (2), which gives us

$$\Re_{n,1}(\varkappa) = \begin{cases} \varkappa - \varsigma_1 & \varsigma_1 \le \varkappa < \varsigma_2, \\ \varsigma_3 - \varkappa & \varsigma_2 \le \varkappa < \varsigma_3, \\ 0 & \text{otherwise}, \end{cases}$$

$$\Re_{n,2}(\varkappa) = \begin{cases} 0 & 0 \le \varkappa < \varsigma_1, \\ \frac{1}{2}(\varkappa - \varsigma_1)^2 & \varsigma_1 \le \varkappa < \varsigma_2, \\ \frac{1}{4q^2} - \frac{1}{2}(\varsigma_1 - \varkappa)^2 & \varsigma_2 \le \varkappa < \varsigma_3, \\ \frac{1}{4q^2} & \varsigma_3 \le \varkappa < 1, \end{cases}$$

$$\Re_{n,3}(\varkappa) = \begin{cases} 0 & 0 \le \varkappa < \varsigma_1, \\ \frac{1}{6}(\varkappa - \varsigma_1)^3 & \varsigma_1 \le \varkappa < \varsigma_2, \\ \frac{1}{4q^2}(\varkappa - \varsigma_2) + \frac{1}{6}(\varsigma_3 - \varkappa)^3 & \varsigma_2 \le \varkappa < \varsigma_3, \\ \frac{1}{4q^2}(\varkappa - \varsigma_2) & \varsigma_3 \le \varkappa < 1, \end{cases} \tag{7}$$

$$\Re_{n,2}(1) = \begin{cases} \frac{1}{2} & \text{if} \quad n = 1, \\ \frac{1}{4q^2} & \text{if} \quad n > 1, \end{cases}$$

$$\Re_{n,3}(1) = \begin{cases} \frac{1}{6} & \text{if} \quad n = 1, \\ \frac{1}{4q^2}(1 - \varsigma_2) & \text{if} \quad n > 1, \end{cases} \tag{8}$$

$$\Re_{n,4}(1) = \begin{cases} \frac{1}{24} & \text{if} \quad n = 1, \\ \frac{1}{4q^2}(1 - \varsigma_2)^2 + \frac{1}{192q^4} & \text{if} \quad n > 1, \end{cases}$$

where Equation (3) defines ς_1, ς_2, ς_3, and m. Furthermore, we need to find:

$$\int_0^1 \psi(\varkappa) \Re_{n,2}(\mathfrak{t})\, d\mathfrak{t}, \tag{9}$$

Consider a function $\psi(\varkappa)$ is provided. Evaluating the integral in Equation (9) is straightforward.

The method's complexity is linear with respect to the number of collocation points due to the sparsity of Haar wavelet basis functions. Compared to global spectral methods, the Haar method has lower memory requirements and avoids large, dense matrix systems.

3. Proposed methodology for 1D and 2D problems

3.1. 1D problem with one integral BC

Consider the 1D equation[40] as follows :

$$\frac{\partial s}{\partial \mathfrak{t}} = \gamma \frac{\partial^2 s}{\partial \varkappa^2} + f(\varkappa, \mathfrak{t}), \quad 0 < \varkappa < 1, \quad 0 < \mathfrak{t} \le T, \tag{10}$$

with the initial, Dirichlet boundary, nonlocal integral boundary conditions

$$s(\varkappa, 0) = \Re(\varkappa), \quad 0 \le \varkappa \le 1, \tag{11}$$

$$s(0, \mathfrak{t}) = g(\mathfrak{t}), \quad 0 \le \mathfrak{t} \le T, \tag{12}$$

$$\int_0^1 \vartheta(\varkappa) s(\varkappa, \mathfrak{t})\, d\varkappa = m(\mathfrak{t}). \tag{13}$$

Where $f(\varkappa, \mathfrak{t})$, $\Re(\varkappa)$, $g(\mathfrak{t})$, $\vartheta(\varkappa)$, and $m(\mathfrak{t})$ are known functions, and the constant γ is also known. Let us consider the following approximation using Haar wavelets:

$$\frac{\partial^2 s}{\partial \varkappa^2} = \sum_{i=1}^{2M} \mu_i h_i(\varkappa). \tag{14}$$

After integrating Equation (14) twice from 0 to $\varkappa$, calculate $\frac{\partial s(0,\mathfrak{t})}{\partial \varkappa}$ by substituting $\varkappa$ with 1. Incorporate this result back into the expression for s by rearranging its terms, which results in the following matrix representation of s.

$$\mathbf{s} = (\mathbf{1} - \mathbf{L})\, s(0,\mathfrak{t}) + \mathbf{L} s(1,\mathfrak{t}) + \left(\mathfrak{R}_2 - \mathbf{L}\mathfrak{R}^T\right)\boldsymbol{\mu}, \tag{15}$$

where

$$\mathbf{L} = [\varkappa_1, \varkappa_2, ..., \varkappa_{2M}]^T, \quad \mathbf{1} = [1, 1, ..., 1]^T,$$
$$\boldsymbol{\mu} = [\mu_1, \mu_2, ..., \mu_{2M}]^T,$$
$$\mathfrak{R} = \left[\Re_{1,2}(1), \quad \Re_{2,2}(1), \quad ... \quad , \Re_{2M,2}(1)\right]^T,$$
$$\mathfrak{R}_2 = \begin{bmatrix} \Re_{1,2}(\varkappa_1) & \Re_{2,2}(\varkappa_1) & ... & \Re_{2M,2}(\varkappa_1) \\ \Re_{1,2}(\varkappa_2) & \Re_{2,2}(\varkappa_2) & ... & \Re_{2M,2}(\varkappa_2) \\ \vdots & \vdots & \ddots & \vdots \\ \Re_{1,2}(\varkappa_{2M}) & \Re_{2,2}(\varkappa_{2M}) & ... & \Re_{2M,2}(\varkappa_{2M}) \end{bmatrix}.$$

To determine $s(1,\mathfrak{t})$, we multiply $\vartheta(\varkappa)$ by the Equation (15) and integrate from 0 to 1 with respect to $\varkappa$. This process involves incorporating the nonlocal integral boundary condition. Subsequently, we substitute the value of $s(1,\mathfrak{t})$ obtained back into Equation (15) and apply the boundary condition given in Equation (12) to derive the approximation for $\mathbf{s}$.

$$\mathbf{s} = (\mathbf{1} - \mathbf{L})\, g(\mathfrak{t}) + \left(\frac{\mathbf{L}}{B_2} m(\mathfrak{t})\right) + \left(\frac{\mathbf{L} B_1}{B_2} g(\mathfrak{t})\right) + \left(\mathfrak{R}_2 - \frac{\mathbf{L}}{B_2}\mathfrak{R}_\vartheta^T\right)\boldsymbol{\mu}, \tag{16}$$

where

$$B_1 = \int_0^1 \vartheta(\varkappa)(1-\varkappa)\, d\varkappa, B_2 = \int_0^1 \vartheta(\varkappa)\varkappa\, d\varkappa,$$

and

$$\mathfrak{R}_\vartheta = \int_0^1 \vartheta(\mathbf{L})\mathfrak{R}\, d\varkappa.$$

The time increment is denoted by $\Delta\mathfrak{t}$. The discrete time instances are represented as $\mathfrak{t}_n = \mathfrak{t}_0 + n \cdot \Delta\mathfrak{t}$, where $\mathfrak{t}_0$ marks the initial time and $\mathfrak{t}_n$ denotes the time at each discrete step. For the time interval $[\mathfrak{t}_0, \mathfrak{t}]$, Euler's formula provides an approximation of the time evolution.

$$\frac{\partial s(\varkappa,\mathfrak{t})}{\partial \mathfrak{t}} \approx \frac{s(\varkappa,\mathfrak{t}) - s(\varkappa,\mathfrak{t}_0)}{\Delta\mathfrak{t}}. \tag{17}$$

Equations (10), (14), and (17) yield the following:

$$\frac{s(\mathbf{L},\mathfrak{t}) - s(\mathbf{L},\mathfrak{t}_0)}{\Delta\mathfrak{t}} = \gamma\mathbf{H}\boldsymbol{\mu} + f(\mathbf{L},\mathfrak{t}), \tag{18}$$

where

$$\mathbf{H} = \begin{bmatrix} h_1(\varkappa_1) & h_2(\varkappa_1) & ... & h_{2M}(\varkappa_1) \\ h_1(\varkappa_2) & h_2(\varkappa_2) & ... & h_{2M}(\varkappa_2) \\ \vdots & \vdots & \ddots & \vdots \\ h_1(\varkappa_{2M}) & h_2(\varkappa_{2M}) & ... & h_{2M}(\varkappa_{2M}) \end{bmatrix}.$$

By applying Equation (16) to Equation (18), we obtain:

$$\left(\mathfrak{R}_2 - \frac{\mathbf{L}}{B_2}\mathfrak{R}_\vartheta^T - \gamma\Delta\mathfrak{t}\mathbf{H}\right)\boldsymbol{\mu} = s(\mathbf{L},\mathfrak{t}_0) + \Delta\mathfrak{t} f(\mathbf{L},\mathfrak{t}) - \left((\mathbf{1}-\mathbf{L})\, g(\mathfrak{t}) + \left(\frac{\mathbf{L}}{B_2} m(t)\right) + \left(\frac{\mathbf{L}B_1}{B_2} g(\mathfrak{t})\right)\right). \tag{19}$$

We need to find the parameter $\boldsymbol{\mu}$ from this set of equations. In the approximate solution given by Equation (16), $\boldsymbol{\mu}$ is subsequently introduced, providing an approximate solution to problem (10).

3.2. 1D problem with two integrals BC

Now, consider the one-dimensional time-dependent diffusion equation [41] provided below:

$$\frac{\partial s}{\partial \mathfrak{t}} = \gamma\frac{\partial^2 s}{\partial \varkappa^2} + f(\varkappa,\mathfrak{t}), 0 < \varkappa < 1, 0 < \mathfrak{t} \le T, \tag{20}$$

having the initial condition defined as:

$$s(\varkappa, 0) = \Re(\varkappa), \quad 0 \le \varkappa \le 1, \tag{21}$$

and in accordance with the nonlocal integral boundary condition:

$$s(0,\mathfrak{t}) = D_1(\mathfrak{t}) + g_1(\mathfrak{t}), \quad 0 < \mathfrak{t} \le T, \tag{22}$$
$$s(1,\mathfrak{t}) = D_2(\mathfrak{t}) + g_2(\mathfrak{t}), \quad 0 < \mathfrak{t} \le T, \tag{23}$$

where

$$D_1(\mathfrak{t}) = \int_0^1 \alpha(\varkappa) s(\varkappa,\mathfrak{t})\, d\varkappa,$$
$$D_2(\mathfrak{t}) = \int_0^1 \vartheta(\varkappa) s(\vartheta,\mathfrak{t})\, d\varkappa,$$

and the functions $f(\varkappa,\mathfrak{t})$, $\Re(\varkappa)$, $\alpha(\varkappa)$, $\vartheta(\varkappa)$, $g_1(\varkappa)$, $g_2(\varkappa)$, and γ are known. After approximating the solution using Equation (15) and incorporating the boundary conditions from Equations (22) and (23), we obtain:

$$\mathbf{s} = (\mathbf{1} - \mathbf{L})\left(D_1(\mathfrak{t}) + g_1(\mathfrak{t})\right) + \mathbf{L}(D_2(\mathfrak{t}) + g_2(\mathfrak{t})) + \left(\mathfrak{R}_2 - \mathbf{L}\mathfrak{R}^T\right)\boldsymbol{\mu}. \tag{24}$$

After multiplying $\alpha(\mathbf{L})$ by Equation (24) and integrating between 0 and 1, we obtain:

$$\begin{aligned} D_1(\mathfrak{t}) =&(D_1(\mathfrak{t}) + g_1(\mathfrak{t})) \int_0^1 \alpha(\mathbf{L}) \, (\mathbf{1} - \mathbf{L}) \; d\varkappa + \\ & (D_2(\mathfrak{t}) + g_2(\mathfrak{t})) \int_0^1 \alpha(\mathbf{L}) \mathbf{L} \, d\varkappa + \\ & \int_0^1 \alpha(\mathbf{L}) \left(\mathfrak{R}_2 - \mathbf{L}\mathfrak{R}^T \right) \; d\varkappa \boldsymbol{\mu}. \end{aligned} \tag{25}$$

Similarly,

$$\begin{aligned} D_2(\mathfrak{t}) =&(D_1(\mathfrak{t}) + g_1(\mathfrak{t})) \int_0^1 \vartheta(\mathbf{L}) \, (\mathbf{1} - \mathbf{L}) \; d\varkappa + \\ & (D_2(\mathfrak{t}) + g_2(\mathfrak{t})) \int_0^1 \vartheta(\mathbf{L}) \mathbf{L} \, d\varkappa \\ & + \int_0^1 \vartheta(\mathbf{L}) \left(\mathfrak{R}_2 - \mathbf{L}\mathfrak{R}^T \right) \; d\varkappa \boldsymbol{\mu}. \end{aligned} \tag{26}$$

From Equations (25) and (26), the values of $D_1(t)$ and $D_2(t)$ are calculated:

$$\begin{aligned} D_1(\mathfrak{t}) = & \frac{1}{m_1(1-B_1)} \Bigg(g_1(\mathfrak{t}) \left(B_1 + \frac{B_2 E_1}{1-E_2} \right) + \\ & g_2(\mathfrak{t}) \left(B_2 + \frac{B_2 E_2}{1-E_2} \right) + \left(\mathfrak{R}_\vartheta + \frac{B_2}{1-E_2} \mathfrak{R}_\alpha - \right. \\ & \left. B_2 \mathfrak{R} \left(1 + \frac{E_2}{1-E_2} \right) \right) \boldsymbol{\mu}, \\ D_2(\mathfrak{t}) = & \frac{1}{m_1(1-E_2)} \Bigg(E_1 g_1(\mathfrak{t}) \left(1 + \frac{B_1}{1-B_1} \right) + \\ & g_2(\mathfrak{t}) \left(E_2 + \frac{B_2 E_1}{1-B_1} \right) + \left(\mathfrak{R}_\alpha + \frac{E_1}{1-B_1} \mathfrak{R}_\vartheta - \right. \\ & \left. \mathfrak{R} \left(E_2 + \frac{E_1 B_2}{1-B_1} \right) \right) \boldsymbol{\mu}, \end{aligned} \tag{27}$$

where

$$\begin{aligned} & B_1 = \int_0^1 \vartheta(\varkappa)(1-\varkappa) \, d\varkappa, B_2 = \int_0^1 \vartheta(\varkappa) \varkappa \, d\varkappa, \\ & E_1 = \int_0^1 \alpha(\varkappa)(1-\varkappa) \, d\varkappa, E_2 = \int_0^1 \alpha(\varkappa) \varkappa \, d\varkappa, \\ & \rho_\alpha = \int_0^1 \alpha(\varkappa) \Re \, d\varkappa, \qquad \rho_\vartheta = \int_0^1 \vartheta(\varkappa) \Re \, d\varkappa, \\ & m_1 = 1 - \frac{B_2 E_1}{(1-B_1)(1-E_1)}. \end{aligned} \tag{28}$$

$$\begin{aligned} \mathbf{s}(\mathbf{L}, \mathfrak{t}) =& (1-\mathbf{L}) g_1(\mathfrak{t}) + \mathbf{L} g_2(\mathfrak{t}) + \frac{1-\mathbf{L}}{m_1(1-B_1)} \\ & \Bigg(g_1(\mathfrak{t}) \left(B_1 + \frac{B_2 E_1}{1-E_2} \right) + g_2(\mathfrak{t}) \left(B_2 \right. \\ & \left. + \frac{B_2 E_2}{1-E_2} \right) + \frac{\mathbf{L}}{m_1(1-E_2)} \Bigg(E_1 g_1(\mathfrak{t}) \\ & \left(1 + \frac{B_1}{1-B_1} \right) + g_2(\mathfrak{t}) \left(E_2 + \frac{B_2 E_1}{1-B_1} \right) \Bigg) \\ & + \Bigg(\mathfrak{R} - \mathbf{L}\mathfrak{R}^T + \frac{1-\mathbf{L}}{m_1(1-B_1)} \Bigg(\mathfrak{R}_\vartheta + \\ & \frac{B_2}{1-E_2} \mathfrak{R}_\alpha - B_2 \mathfrak{R} \left(1 + \frac{E_2}{1-E_2} \right) \Bigg)^T \Bigg) \boldsymbol{\mu} \\ & + \Bigg(\frac{\mathbf{L}}{m_1(1-E_2)} \Bigg(\mathfrak{R}_\alpha + \frac{E_1}{1-B_1} \mathfrak{R}_\vartheta \\ & - \mathfrak{R} \left(E_2 + \frac{E_1 B_2}{1-B_1} \right) \Bigg)^T \Bigg) \boldsymbol{\mu}. \end{aligned} \tag{29}$$

From Equations (17) and (20), we obtain:

$$\frac{\mathbf{s}(\mathbf{L}, \mathfrak{t}) - s(\mathbf{L}, \mathfrak{t}_0)}{\Delta \mathfrak{t}} = \gamma \mathbf{H} \boldsymbol{\mu} + f(\mathbf{L}, \mathfrak{t}). \tag{30}$$

Inserting from Equation (29) the value of $s(\mathbf{L}, t)$ in Equation (30).

$$\begin{aligned} & \Bigg(\mathfrak{R} - \mathbf{L}\mathfrak{R}^T - \gamma \Delta \mathfrak{t} \mathbf{H} + \frac{1-\mathbf{L}}{m_1(1-B_1)} \Bigg(\mathfrak{R}_\vartheta \frac{B_2}{1-E_2} \mathfrak{R}_\alpha \\ & - B_2 \mathfrak{R} \left(1 + \frac{E_2}{1-E_2} \right)^T \boldsymbol{\mu} + \Bigg(\frac{\mathbf{L}}{m_1(1-E_2)} \left(\mathfrak{R}_\alpha \right. \\ & \left. + \frac{E_1}{1-B_1} \mathfrak{R}_\vartheta - \mathfrak{R} \left(E_2 + \frac{E_1 B_2}{1-B_1} \right)^T \boldsymbol{\mu}, \right. \\ = & - \Bigg((1-\mathbf{L}) g_1(\mathfrak{t}) + \mathbf{L} g_2(\mathfrak{t}) + \frac{1-\mathbf{L}}{m_1(1-B_1)} \Bigg(g_1(\mathfrak{t}) \\ & \left(B_1 + \frac{B_2 E_1}{1-E_2} \right) + g_2(\mathfrak{t}) \left(B_2 + \frac{B_2 E_2}{1-E_2} \right) \Bigg) \Bigg) \\ & - \Bigg(\frac{\mathbf{L}}{m_1(1-E_2)} \Bigg(E_1 g_1(\mathfrak{t}) \left(1 + \frac{B_1}{1-B_1} \right) + \\ & g_2(\mathfrak{t}) \left(E_2 + \frac{B_2 E_1}{1-B_1} \right) \Bigg) \Bigg) + s(\mathbf{L}, \mathfrak{t}_0) + \Delta \mathfrak{t} f(\mathbf{L}, \mathfrak{t}). \end{aligned} \tag{31}$$

Computing $\boldsymbol{\mu}$ by solving this system of equations. Next, substitute $\boldsymbol{\mu}$ in Equation (29), the approximate solution.

3.3. 2D problem with integral BC

Consider,[42]

$$\begin{aligned} \frac{\partial s}{\partial \mathfrak{t}} =& \gamma \left(\frac{\partial^2 s}{\partial \varkappa^2} + \frac{\partial^2 s}{\partial \mathfrak{y}^2} \right) + f(\varkappa, \mathfrak{y}, \mathfrak{t}), \\ & 0 < \varkappa < 1, \quad 0 < \mathfrak{y} < 1, \end{aligned} \tag{32}$$

which is accompanied by the nonlocal integral boundary conditions:

$$s(0,\mathfrak{y},\mathfrak{t}) = \alpha_1 \int_0^1 \alpha(\varkappa) s(\varkappa,\mathfrak{y},\mathfrak{t})\, d\varkappa + \Im_1(\mathfrak{y},\mathfrak{t}), \quad 0<\mathfrak{y}<1, \quad 0<\mathfrak{t}\le T, \tag{33}$$

$$s(1,\mathfrak{y},\mathfrak{t}) = \alpha_2 \int_0^1 \vartheta(\varkappa) s(\varkappa,\mathfrak{y},\mathfrak{t})\, d\varkappa + \Im_2(\mathfrak{y},\mathfrak{t}), \quad 0<\mathfrak{y}<1, \quad 0<\mathfrak{t}\le T. \tag{34}$$

Dirichlet boundary conditions and the initial condition are expressed as:

$$s(\varkappa,0,\mathfrak{t}) = \Im_3(\varkappa,\mathfrak{t}), 0<\varkappa<1, 0<\mathfrak{t}\le T, \tag{35}$$
$$s(\varkappa,1,\mathfrak{t}) = \Im_4(\varkappa,\mathfrak{t}), 0<\varkappa<1, 0<\mathfrak{t}\le T, \tag{36}$$
$$s(\varkappa,\mathfrak{y},0) = \phi(\varkappa,\mathfrak{y}), 0\le\varkappa\le 1, 0\le\mathfrak{y}\le 1. \tag{37}$$

where $f(\varkappa,\mathfrak{y},\mathfrak{t})$, $\alpha(\varkappa)$, $\vartheta(\varkappa)$, $\Im_1(\mathfrak{y})$, $\Im_2(\varkappa)$, $\Im_3(\varkappa)$, $\Im_4(\mathfrak{y})$ are known smooth functions, parameters α_1 and α_2 are given, while the function $s(\varkappa,\mathfrak{y},\mathfrak{t})$ is unknown. It is assumed that there is mutual compatibility between the Dirichlet boundary conditions (Equations (35) and (36)) and the nonlocal integral boundary conditions (Equations (33) and (34)).

For the mixed fourth-order derivative, let us investigate the Haar wavelet approximation:

$$\frac{\partial^4 s}{\partial\varkappa^2\partial\mathfrak{y}^2} = \sum_{i=1}^{2M}\sum_{j=1}^{2M} \mu_{i,j} h_i(\varkappa) h_j(\mathfrak{y}). \tag{38}$$

We derive this by performing two successive partial integrations of Equation (38) with respect to $\varkappa$, from 0 to $\varkappa$.

$$\frac{\partial^2 s}{\partial\mathfrak{y}^2} = \frac{\partial^2 s(0,\mathfrak{y})}{\partial\mathfrak{y}^2} + \varkappa\frac{\partial^3 s(0,\mathfrak{y})}{\partial\varkappa\partial\mathfrak{y}^2} + \sum_{i=1}^{2M}\sum_{j=1}^{2M} \mu_{i,j} h_j(\mathfrak{y}) \int_0^{\varkappa}\int_0^{\varkappa} h_i(\varkappa)\, d\varkappa\, d\varkappa. \tag{39}$$

In light of that, we consider:

$$\frac{\partial^3 s(0,\mathfrak{y})}{\partial\varkappa\partial\mathfrak{y}^2} = \sum_{j=1}^{2M} \omega_j h_j(\mathfrak{y}),$$
$$\frac{\partial^2 s(0,\mathfrak{y})}{\partial\mathfrak{y}^2} = \sum_{j=1}^{2M} \zeta_j h_j(\mathfrak{y}), \tag{40}$$
$$\rho_{i,2}(\varkappa) = \int_0^{\varkappa}\int_0^{\varkappa} h_i(\varkappa)\, d\varkappa\, d\varkappa.$$

It is possible to write Equation (40) with the additions of Equation (39):

$$\frac{\partial^2 s(\varkappa_k,\mathfrak{y}_l)}{\partial\mathfrak{y}^2} = \sum_{j=1}^{2M} \zeta_j h_j(\mathfrak{y}_l) + \varkappa_k \sum_{j=1}^{2M} \omega_j h_j(\mathfrak{y}_l) + \sum_{i=1}^{2M}\sum_{j=1}^{2M} \mu_{i,j}\rho_{i,2}(\varkappa_k) h_j(\mathfrak{y}_l), \tag{41}$$

where the collocation points are:

$$\varkappa_k = \frac{k-1/2}{2M},\ k=1,2,\ldots,2M, \qquad \mathfrak{y}_l = \frac{l-1/2}{2M},\ l=1,2,\ldots,2M. \tag{42}$$

The Equation (41) in matrix form can be represented as:

$$\mathbf{s}_{\mathfrak{y}\mathfrak{y}} = (\mathbf{1}\otimes\mathbf{H})\boldsymbol{\zeta} + (\mathbf{L}\otimes\mathbf{H})\boldsymbol{\omega} + (\mathfrak{R}_2\otimes\mathbf{H})\boldsymbol{\mu}, \tag{43}$$

where as:

$$\mathbf{s}_{\mathfrak{y}\mathfrak{y}} = [\frac{\partial^2 s}{\partial\mathfrak{y}^2}(\varkappa_1,\mathfrak{y}_1), \frac{\partial^2 s}{\partial\mathfrak{y}^2}(\varkappa_1,\mathfrak{y}_2), ..., \frac{\partial^2 s}{\partial\mathfrak{y}^2}(\varkappa_1,\mathfrak{y}_n), \frac{\partial^2 s}{\partial\mathfrak{y}^2}(\varkappa_2,\mathfrak{y}_1), \frac{\partial^2 s}{\partial\mathfrak{y}^2}(\varkappa_2,\mathfrak{y}_2), ..., \frac{\partial^2 s}{\partial\mathfrak{y}^2}(\varkappa_2,\mathfrak{y}_n), ..., \frac{\partial^2 s}{\partial\mathfrak{y}^2}(\varkappa_n,\mathfrak{y}_1), \frac{\partial^2 s}{\partial\mathfrak{y}^2}(\varkappa_{2M},\mathfrak{y}_2), ..., \frac{\partial^2 s}{\partial\mathfrak{y}^2}(\varkappa_{2M},\mathfrak{y}_{2M})]^T,$$
$$\boldsymbol{\zeta} = [\zeta_1,\zeta_2,...,\zeta_{2M}]^T, \quad \boldsymbol{\omega} = [\omega_1,\omega_2,...,\omega_{2M}]^T,$$
$$\boldsymbol{\mu} = [\mu_{1,1},\mu_{1,2},...,\mu_{1,2M},\mu_{2,1},\mu_{2,2},...,\mu_{2,2M},...,\mu_{2M,1},\mu_{2M,2},...,\mu_{2M,2M}]^T,$$

Following a similar approach, integrating Equation (38) twice with respect to $\mathfrak{y}$ over the interval from 0 to $\mathfrak{y}$:

$$\mathbf{s}_{\varkappa\varkappa} = (\mathbf{H}\otimes\mathbf{1})\boldsymbol{\sigma} + (\mathbf{H}\otimes\mathfrak{y})\boldsymbol{\delta} + (\mathbf{H}\otimes\mathfrak{R}_2)\boldsymbol{\mu}, \tag{44}$$

where

$$\mathfrak{y} = [\mathfrak{y}_1,\mathfrak{y}_2,...,\mathfrak{y}_{2M}]^T,\ \boldsymbol{\sigma} = [\sigma_1,\sigma_2,...,\sigma_{2M}]^T,$$
$$\boldsymbol{\delta} = [\delta_1,\delta_2,...,\delta_{2M}]^T.$$

By integrating Equation (43) twice over the interval from 0 to y, we obtain:

$$\mathbf{s} = (\mathbf{s}(\mathbf{L},0)\otimes\mathbf{1}) + (\mathbf{s}_{\mathfrak{y}}|_{\mathfrak{y}=0}\otimes\mathfrak{y}) + (\mathbf{1}\otimes\mathfrak{R}_2)\boldsymbol{\zeta} + (\mathbf{L}\otimes\mathfrak{R}_2)\boldsymbol{\omega} + (\mathfrak{R}_2\otimes\mathfrak{R}_2)\boldsymbol{\mu}, \tag{45}$$

where

$$\mathbf{s}_{\mathfrak{y}}|_{\mathfrak{y}=0} = [\frac{\partial s}{\partial\mathfrak{y}}(\varkappa_1,0), \frac{\partial s}{\partial\mathfrak{y}}(\varkappa_1,0), ..., \frac{\partial s}{\partial\mathfrak{y}}(\varkappa_1,0), \frac{\partial s}{\partial\mathfrak{y}}(\varkappa_2,0), \frac{\partial s}{\partial\mathfrak{y}}(\varkappa_2,0), ..., \frac{\partial s}{\partial\mathfrak{y}}(\varkappa_2,0), ..., \frac{\partial s}{\partial\mathfrak{y}}(\varkappa_n,0), \frac{\partial s}{\partial\mathfrak{y}}(\varkappa_{2M},0), ..., \frac{\partial s}{\partial\mathfrak{y}}(\varkappa_{2M},0)]^T.$$

Equation (45) makes it simple to get the value of $\mathbf{s}_{\mathfrak{y}}|_{\mathfrak{y}=0}$. To do this, simply substitute $\mathbf{L}$ for $\mathbf{1}$ in Equation (45), find $\mathbf{s}_{\mathfrak{y}}|_{\mathfrak{y}=c}$, and then put this value back in Equation (45). We get:

$$\begin{aligned}\mathbf{s} =&(\mathbf{s}(\mathbf{L},0)\otimes\mathbf{1}) + ((\mathbf{s}(\mathbf{L},\mathbf{d}) - \mathbf{s}(\mathbf{L},0))\otimes\mathfrak{y})\\ &+ \left(\mathbf{1}\otimes\left(\mathfrak{R}_2 - \mathfrak{y}\mathfrak{R}^T\right)\right)\boldsymbol{\zeta} + \left(\mathbf{L}\otimes\left(\mathfrak{R}_2 - \mathfrak{y}\mathfrak{R}^T\right)\right)\boldsymbol{\omega}\\ &+ \left(\mathfrak{R}_2\otimes\left(\mathfrak{R}_2 - \mathfrak{y}\mathfrak{R}^T\right)\right)\boldsymbol{\mu},\end{aligned} \tag{46}$$

where

$$\mathfrak{R} = \begin{bmatrix}\Re_{1,2}(1) & \Re_{2,2}(1) & \ldots & \Re_{2M,2}(1)\end{bmatrix}^T.$$

In the same way, from Equation (44), we derive:

$$\begin{aligned}\mathbf{s} =&(\mathbf{1}\otimes\mathbf{s}(0,\mathfrak{y})) + (\mathbf{L}\otimes(\mathbf{s}(1,\mathfrak{y}) - \mathbf{s}(0,\mathfrak{y})))\\ &+ \left(\left(\mathfrak{R}_2 - \mathbf{L}\mathfrak{R}^T\right)\otimes\mathbf{1}\right)\boldsymbol{\sigma} + \left(\left(\mathfrak{R}_2 - \mathbf{L}\mathfrak{R}^T\right)\otimes\mathfrak{y}\right)\boldsymbol{\delta}\\ &+ \left(\left(\mathfrak{R}_2 - \mathbf{L}\mathfrak{R}^T\right)\otimes\mathfrak{R}_2\right)\boldsymbol{\mu}.\end{aligned} \tag{47}$$

The expression below results from applying the boundary conditions described by Equation (33) to Equation (34) within Equation (46).

$$\begin{aligned}\mathbf{s} =&(\Im_3(\mathbf{L},\mathfrak{t})\otimes\mathbf{1}) + ((\Im_4(\mathbf{L},\mathfrak{t}) - \Im_3(\mathbf{L},\mathfrak{t}))\otimes\mathfrak{y})\\ &+ \left(\mathbf{1}\otimes\left(\mathfrak{R}_2 - \mathfrak{y}\mathfrak{R}^T\right)\right)\boldsymbol{\zeta} + \left(\mathbf{L}\otimes\left(\mathfrak{R}_2 - \mathfrak{y}\mathfrak{R}^T\right)\right)\boldsymbol{\omega}\\ &+ \left(\mathfrak{R}_2\otimes\left(\mathfrak{R}_2 - \mathfrak{y}\mathfrak{R}^T\right)\right)\boldsymbol{\mu},\end{aligned} \tag{48}$$

The expressions $\int_0^1 \alpha(\varkappa)s(\varkappa,\mathfrak{y},\mathfrak{t})\,d\varkappa$ and $\int_0^1 \vartheta(\varkappa)s(\varkappa,\mathfrak{y},\mathfrak{t})\,d\varkappa$ can be derived from Equation (48) and are presented as follows:

$$\begin{aligned}\int_0^1 \boldsymbol{\alpha}\mathbf{s}\,d\varkappa =& \left(\int_0^1 \boldsymbol{\alpha}\Im_3(\mathbf{L},\mathfrak{t})\,d\varkappa\otimes\mathbf{1}\right) +\\ &\left(\int_0^1 \boldsymbol{\alpha}(\Im_4(\mathbf{L},\mathfrak{t}) - \Im_3(\mathbf{L},\mathfrak{t}))\,d\varkappa\otimes\mathfrak{y}\right) +\\ &\left(\int_0^1 \boldsymbol{\alpha}\,d\varkappa\otimes\left(\mathfrak{R}_2 - \mathfrak{y}\mathfrak{R}^T\right)\right)\boldsymbol{\zeta} +\\ &\left(\int_0^1 \boldsymbol{\alpha}\mathbf{L}\,d\varkappa\otimes\left(\mathfrak{R}_2 - \mathfrak{y}\mathfrak{R}^T\right)\right)\boldsymbol{\omega} +\\ &\left(\int_0^1 \boldsymbol{\alpha}\mathfrak{R}_2\,d\varkappa\otimes\left(\mathfrak{R}_2 - \mathfrak{y}\mathfrak{R}^T\right)\right)\boldsymbol{\mu},\end{aligned} \tag{49}$$

$$\begin{aligned}\int_0^1 \boldsymbol{\vartheta}\mathbf{s}\,d\varkappa =& \left(\int_0^1 \boldsymbol{\vartheta}\Im_3(\mathbf{L},\mathfrak{t})\,d\varkappa\otimes\mathbf{1}\right) +\\ &\left(\int_0^1 \boldsymbol{\vartheta}(\Im_4(\mathbf{L},\mathfrak{t}) - \Im_3(\mathbf{L},\mathfrak{t}))\,d\varkappa\otimes\mathfrak{y}\right) +\\ &\left(\int_0^1 \boldsymbol{\vartheta}\,d\varkappa\otimes\left(\mathfrak{R}_2 - \mathfrak{y}\mathfrak{R}^T\right)\right)\boldsymbol{\zeta} +\\ &\left(\int_0^1 \boldsymbol{\vartheta}\mathbf{L}\,d\varkappa\otimes\left(\mathfrak{R}_2 - \mathfrak{y}\mathfrak{R}^T\right)\right)\boldsymbol{\omega} +\\ &\left(\int_0^1 \boldsymbol{\vartheta}\mathfrak{R}_2\,d\varkappa\otimes\left(\mathfrak{R}_2 - \mathfrak{y}\mathfrak{R}^T\right)\right)\boldsymbol{\mu},\end{aligned} \tag{50}$$

where

$$\begin{aligned}\boldsymbol{\alpha} &= [\alpha(\varkappa_1),\alpha(\varkappa_2),\alpha(\varkappa_3),...,,\alpha(\varkappa_{2M})]^T,\\ \boldsymbol{\vartheta} &= [\vartheta(\varkappa_1),\vartheta(\varkappa_2),\vartheta(\varkappa_3),...,,\vartheta(\varkappa_{2M})]^T.\end{aligned} \tag{51}$$

The integral boundary conditions, denoted as Equations (33) and (34), result from multiplying α_1 by Equation (49) and α_2 by Equation (50). After substituting these derived expressions into Equation (47) and rearranging, we derive an alternative expression for $\mathbf{s}$.

$$\begin{aligned}\mathbf{s} =& ((\mathbf{1}-\mathbf{L})\otimes\Im_1(\mathfrak{y})) + (\mathbf{L}\otimes\Im_2(\mathfrak{y})) +\\ &\left(\alpha_1(\mathbf{1}-\mathbf{L})\int_0^1 \boldsymbol{\alpha}\Im_3(\mathbf{L},\mathfrak{t})\,d\varkappa\otimes\mathbf{1}\right) +\\ &\left(\mathbf{L}\alpha_2\int_0^1 \boldsymbol{\vartheta}\Im_3(\mathbf{L},\mathfrak{t})\,d\varkappa\otimes\mathbf{1}\right) +\\ &\left((\mathbf{1}-\mathbf{L})\,\alpha_1\int_0^1 \boldsymbol{\alpha}(\Im_4(\mathbf{L},\mathfrak{t}) - \Im_3(\mathbf{L},\mathfrak{t}))\,d\varkappa\otimes\mathfrak{y}\right) +\\ &\left(\mathbf{L}\alpha_2\int_0^1 \boldsymbol{\vartheta}(\Im_4(\mathbf{L},\mathfrak{t}) - \Im_3(\mathbf{L},\mathfrak{t}))\,d\varkappa\otimes\mathfrak{y}\right) +\\ &\left((\mathbf{1}-\mathbf{L})\,\alpha_1\int_0^1 \boldsymbol{\alpha}\,d\varkappa +\right.\\ &(\mathbf{L})\,\alpha_2\int_0^1 \boldsymbol{\vartheta}\,d\varkappa\otimes\left(\mathfrak{R}_2 - \mathfrak{y}\mathfrak{R}^T\right)\boldsymbol{\zeta} +\\ &\left((\mathbf{1}-\mathbf{L})\,\alpha_1\int_0^1 \mathbf{L}\boldsymbol{\alpha}\,d\varkappa +\right.\\ &(\mathbf{L})\,\alpha_2\int_0^1 \mathbf{L}\boldsymbol{\vartheta}\,d\varkappa\otimes\left(\mathfrak{R}_2 - \mathfrak{y}\mathfrak{R}^T\right)\boldsymbol{\omega} +\\ &\left(\left((\mathbf{1}-\mathbf{L})\,\alpha_1\left(\int_0^1 \boldsymbol{\alpha}\mathfrak{R}_2\,d\varkappa\right)^T +\right.\right.\\ &(\mathbf{L})\,\alpha_2\left(\int_0^1 \boldsymbol{\vartheta}\mathfrak{R}_2\,d\varkappa\right)^T\otimes\left(\mathfrak{R}_2 - \mathfrak{y}\mathfrak{R}^T\right) +\\ &\left.\left.\left.\left(\mathfrak{R}_2 - \mathbf{L}\mathfrak{R}^T\right)\otimes\mathfrak{R}_2\right)\right)\boldsymbol{\mu}.\end{aligned} \tag{52}$$

From Equations (17), (44), and (43), we have:

$$\begin{aligned}\frac{s(\mathbf{L},\mathfrak{t})-s(\mathbf{L},\mathfrak{t}_0)}{\Delta\mathfrak{t}} &= \gamma\big((\mathbf{H}\otimes\mathbf{1})\boldsymbol{\sigma}+\\ &(\mathbf{H}\otimes\mathfrak{y})\boldsymbol{\delta}+(\mathbf{1}\otimes\mathbf{H})\boldsymbol{\zeta}+(\mathbf{L}\otimes\mathbf{H})\boldsymbol{\omega}+\\ &((\mathfrak{R}_2\otimes\mathbf{H})+(\mathbf{H}\otimes\mathfrak{R}_2))\boldsymbol{\mu}\big)+f(\mathbf{L},\mathfrak{t}).\end{aligned} \tag{53}$$

According to Equation (53), a system of $4M^2$ equations involving $4M^2+8M$ unknowns is produced by Equation (52). By setting Equations (48) equal to (52) and substituting $\varkappa=0$, $\varkappa=1$, $\mathfrak{y}=0$, and $\mathfrak{y}=1$, we derive another system of $8M$ equations with $4M^2+8M$ unknowns. The Haar coefficients for the unknowns $\boldsymbol{\mu}$, $\boldsymbol{\zeta}$, $\boldsymbol{\omega}$, $\boldsymbol{\sigma}$, and $\boldsymbol{\delta}$ are determined by solving both sets of equations simultaneously. These coefficients subsequently substitute the solution of the given problem either in Equation (48) or Equation (52).

4. Numerical results and discussion

In this section, we present numerical experiments on various one- and two-dimensional parabolic PDEs with integral boundary conditions using an effective Haar wavelet collocation method. These experiments indicate that the proposed method yields accurate solutions, particularly when the parameters of the integral boundary conditions are negative.

Problem 1. *Consider the problem presented in Equation (10), where the functions are defined as follows:*

$$\begin{aligned}f(\varkappa,\mathfrak{t}) &= -e^{(\mathfrak{t}+\varkappa)}(\gamma-1),\\ \Re(\varkappa) &= e^{\varkappa},\\ g(\mathfrak{t}) &= e^{\mathfrak{t}},\\ m(\mathfrak{t}) &= \int_0^1 \vartheta(\mathfrak{x})e^{\mathfrak{x}+\mathfrak{t}}dx,\end{aligned} \tag{54}$$

with the exact solution:

$$s(\varkappa,\mathfrak{t})=e^{\varkappa+\mathfrak{t}}. \tag{55}$$

Table 1 presents the numerical results for Test Problem 1 obtained using the proposed Haar wavelets method. The parameter values used in Table 1 are $\vartheta=-50$, $\gamma=2$, and $T=1$. To evaluate the effect of different parameters on the accuracy of the proposed method, various values of M and dt are considered, specifically $M=4,8,16,32,64$ and $dt=0.05,0.005,0.0005$. These results were generated with different values of M and $d\mathfrak{t}$. The table indicates that even with a coarse selection of collocation points, the method achieves satisfactory accuracy, which improves as M increases and $d\mathfrak{t}$ decreases. Additionally, Figures 1-2 depict the method's performance in terms of L_∞. It is evident from these figures that the method's accuracy remains relatively stable regardless of the increase in collocation points M or changes in ϑ.

Table 1. The numerical results generated using Haar wavelets for Test Problem 1 with parameters $\vartheta=1$, $T=1$, and $\gamma=1$

	$d\mathfrak{t}=0.0005$	$d\mathfrak{t}=0.005$	$d\mathfrak{t}=0.05$
$M\ \backslash L_\infty$			
4	2.4349e − 04	2.1402e − 04	2.1902e − 03
8	2.1342e − 05	2.6395e − 04	2.3891e − 03
16	2.2141e − 05	2.5393e − 04	2.2890e − 03
32	2.5340e − 05	2.3393e − 04	2.1889e − 03
64	2.6340e − 05	2.1393e − 04	2.5889e − 03

Table 2. The numerical results generated using Haar wavelets for Test Problem 2 with parameters $\vartheta=-50$, $\gamma=2$, and $T=1$

	$d\mathfrak{t}=0.0005$	$d\mathfrak{t}=0.005$	$d\mathfrak{t}=0.05$
$M\ \backslash L_\infty$			
4	3.5616e − 04	4.2593e − 04	7.5728e − 03
8	3.7148e − 05	6.8963e − 04	6.8353e − 03
16	6.2383e − 05	7.7280e − 04	7.8397e − 03
32	7.6387e − 05	8.5852e − 04	7.6956e − 03
64	8.5374e − 05	8.7694e − 04	8.7802e − 03

Problem 2. *Consider the problem presented in Equation (10), where the functions are defined as follows[40]:*

$$\begin{aligned}\Re(\varkappa) &= \cos\left(\frac{\pi}{2}\varkappa\right),\\ g(\mathfrak{t}) &= e^{\frac{-\pi^2}{4}\mathfrak{t}},\\ m(\mathfrak{t}) &= \frac{2}{\pi}\left(e^{\frac{-\pi^2}{4}\mathfrak{t}}\right).\end{aligned} \tag{56}$$

The theoretical solution of this problem is:

$$s(\varkappa,\mathfrak{t})=e^{\frac{-\pi^2}{4}\mathfrak{t}}\cos\left(\frac{\pi}{2}\varkappa\right). \tag{57}$$

Table 2 presents the numerical results of the Haar wavelet method for Test Problem 2 with varying values of M and $d\mathfrak{t}$. The parameter values used in Table 2 are $\vartheta=1$, $\gamma=1$, and $T=1$. Furthermore, different values of M ($M=4,8,16,32,64$) and $d\mathfrak{t}$ ($d\mathfrak{t}=0.05,0.005,0.0005$) are considered to assess their influence on the accuracy of the proposed method. The accuracy of the method improves as M increases and the

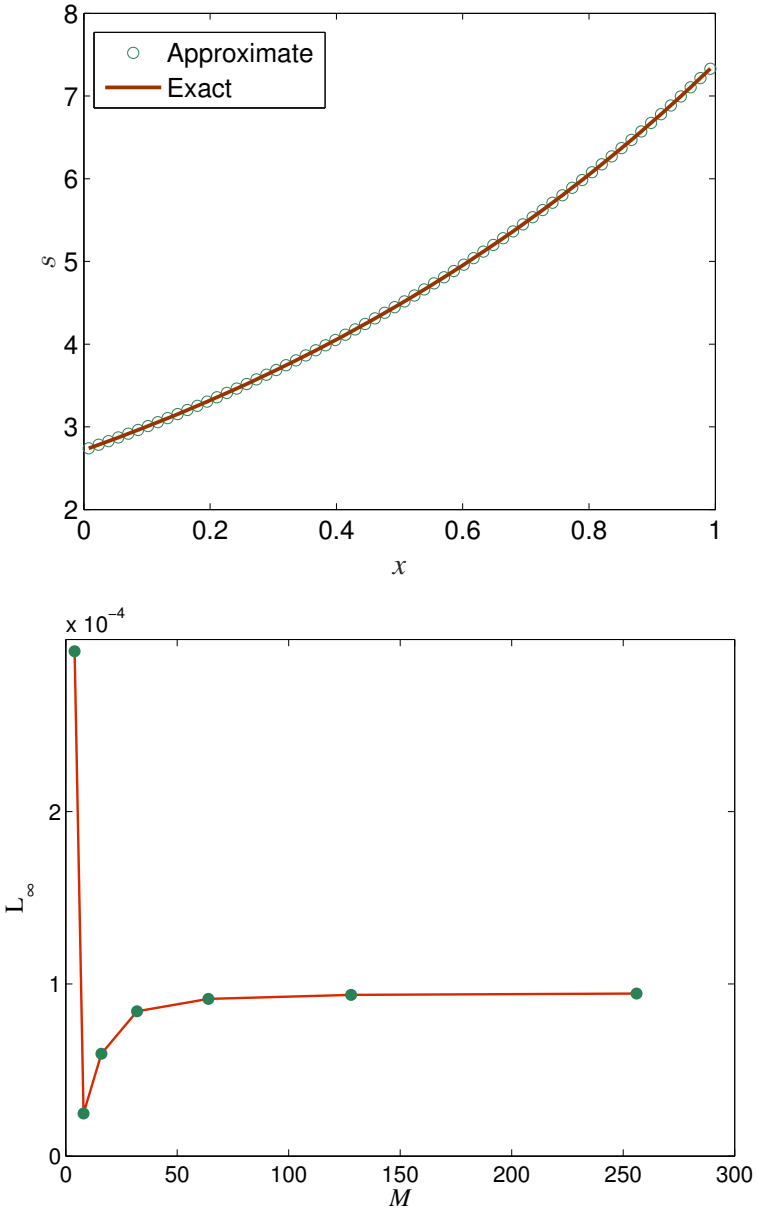

Figure 1. Comparison of exact and approximate and the L_∞ error norm with respect to M using Haar wavelets for Test Problem 1

time step size $d\mathfrak{t}$ decreases. Table 2 presents a comparison of the numerical results obtained using the proposed method with those from other numerical methods. The results indicate that the proposed method achieves improved accuracy.

Figure 3 illustrates the connection between ϑ and the method's accuracy as measured by the L_∞ norm. The data reveal that as ϑ rises from -50 to -10, the error decreases, signifying an improvement in the numerical solution's precision.

Table 3. A comparison of Haar wavelets with the results in[40] at $\vartheta = 1$, $\gamma = 1$, $T = 1$ for Test Problem 2

$d\mathfrak{t}$	HWM	Implicit	Galerkin	Keller-Box	RKC	Saulyev I
0.0500	1.49e − 03	9.1e − 03	9.9e − 02	9.4e − 02	9.8e − 02	9.6e − 03
0.0250	7.46e − 04	2.3e − 03	3.0e − 02	2.4e − 02	3.7e − 02	2.5e − 03
0.0100	2.98e − 04	3.8e − 04	4.9e − 03	4.1e − 03	6.1e − 03	3.9e − 04
0.0050	1.49e − 04	9.4e − 05	1.2e − 03	1.0e − 03	1.5e − 03	9.6e − 05
0.0025	7.46e − 05	2.3e − 05	3.1e − 04	2.5e − 04	3.5e − 04	2.5e − 05
0.0010	2.98e − 05	4.1e − 05	5.0e − 05	4.0e − 05	6.0e − 05	4.3e − 06

However, when ϑ reaches 20, there is a notable increase in the L_∞ norm, which is considerably higher than the error observed for the other ϑ values. Where in Figure 4, the relationship between ϑ and condition number κ is given. It can be seen from the figure that the condition number increases slightly when ϑ increases toward 50 from 0.

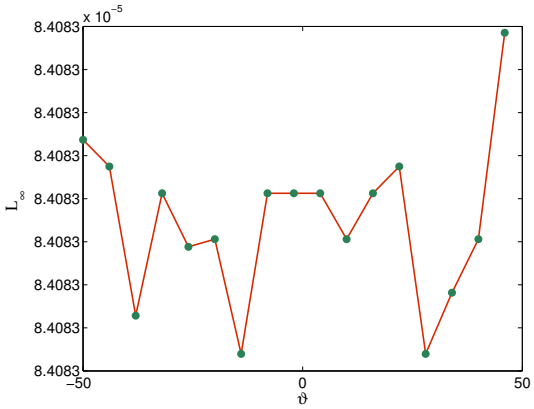

Figure 2. Comparison of the L_∞ error norm with respect to ϑ using Haar wavelets for Test Problem 1

Problem 3. *Consider the problem described by Equations (20 - 23), where the functions are specified as follows:*

$$f(\varkappa, \mathfrak{t}) = \frac{-2(\varkappa^2 + \mathfrak{t} + 1)}{(\mathfrak{t}+1)^3},$$

$$\Re(\varkappa) = \varkappa^2,$$

$$g_1(\mathfrak{t}) = -\int_0^1 \alpha(\varkappa) \left(\frac{\varkappa}{\mathfrak{t}+1}\right)^2 dx,$$

$$g_2(\mathfrak{t}) = \left(\frac{1}{\mathfrak{t}+1}\right)^2 - \int_0^1 \vartheta(\varkappa) \left(\frac{\varkappa}{\mathfrak{t}+1}\right)^2 dx, \quad (58)$$

where, $\alpha(\varkappa) = 1$ *and* $\vartheta(\varkappa) = 1$. *The theoretical solution of this problem is:*

$$s(\varkappa, \mathfrak{t}) = \left(\frac{\varkappa}{\mathfrak{t}+1}\right)^2. \quad (59)$$

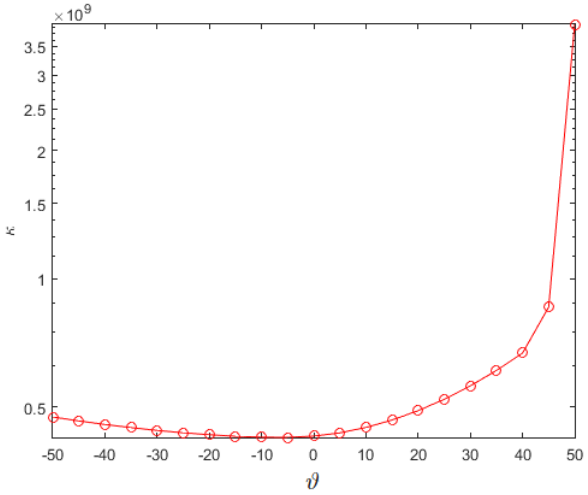

Figure 4. Comparison of the ϑ versus κ using Haar wavelets for Test Problem 2

The numerical outcomes of the suggested Haar wavelet approach for Test Problem 3 are shown in Figure 5. The figure shows that the accuracy improves as the number of collocation points M increases. The method achieves good accuracy even with coarse nodes while maintaining a small time step.

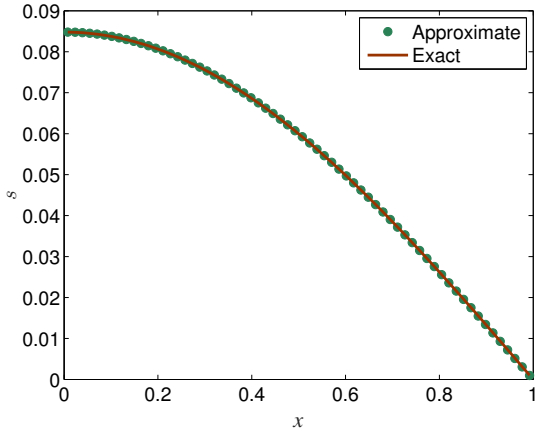

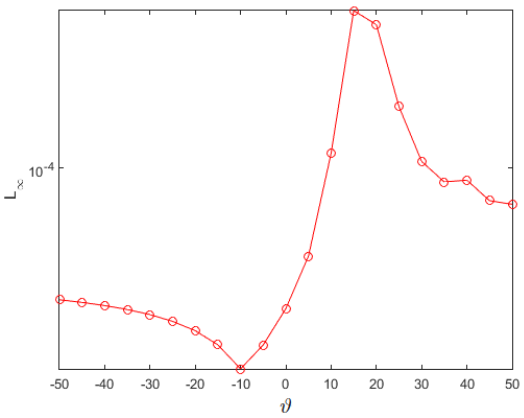

Figure 3. Comparison of exact and approximate and the L_∞ error norm versus ϑ using Haar wavelets for Test Problem 2

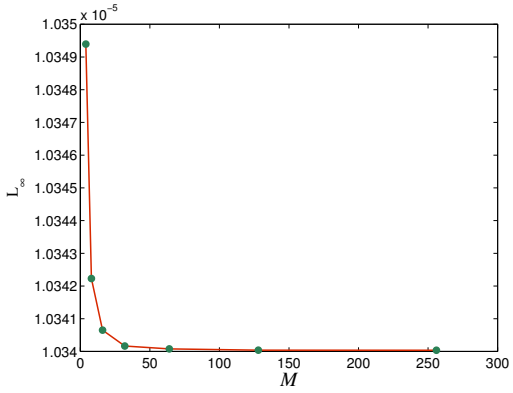

Figure 5. Comparison of the L_∞ error norm versus M using Haar wavelets for Test Problem 3

Problem 4. *Consider the steady-state problem of Equation (32), where the functions are specified as follows:*

$$\begin{aligned} f(\varkappa,\mathfrak{y}) &= 2e^{\varkappa+\mathfrak{y}},\\ \Im_1(\mathfrak{y}) &= e^{\mathfrak{y}} - \int_0^1 \vartheta(\varkappa)e^{\varkappa+\mathfrak{y}}d\varkappa,\\ \Im_2(\mathfrak{y}) &= e^{\mathfrak{y}+1} - \int_0^1 \alpha(\varkappa)e^{\varkappa+\mathfrak{y}}d\varkappa,\\ \Im_3(\mathfrak{y}) &= e^{\varkappa},\\ \Im_4(\mathfrak{y}) &= e^{\varkappa+1}, \end{aligned} \tag{60}$$

where the exact solution is:

$$s(\varkappa,\mathfrak{y}) = e^{\varkappa+y}. \tag{61}$$

We select $M = 16$ and $dt = 0.005$, using ϑ values of -10, 0, 2, and 10 to generate numerical results for different values of α, specifically $\alpha = -10, -3, -2, 0, 2, 3$, and 10, as shown in Tables 4 and 5. These tables present the numerical errors and condition numbers for various values of α, demonstrating that only slight variations in the error norm occur when the parameters α and ϑ are varied. In Tables 4 and 5, for $\vartheta = -10$ and $\vartheta = 0$, the L_∞ error norms and condition numbers show minor fluctuations as α changes, with a slight increase in error as α moves further away from zero.

Tables 4 and 5 emphasize the importance of selecting an appropriate parameter ϑ to obtain accurate solutions when using the Haar wavelet method for 2D integral problems. Figure 6 presents a comparison between the exact solution and the numerical solution obtained with the proposed method.

Negative values of α and ϑ influence the integral boundary conditions in a way that introduces a smoothing or damping effect on the solution, particularly near the domain boundaries. This regularizing behavior reduces the influence of sharp gradients or discontinuities, which often challenge numerical methods. The Haar wavelet basis, with its compact support and localized resolution, is particularly effective in capturing these smoother variations. Additionally, the nonlocal nature of the boundary conditions, combined with negative parameter values, tends to suppress high-frequency components, thereby enhancing the accuracy and stability of the Haar wavelet collocation method in such scenarios.

Table 4. The numerical results generated using Haar wavelets for Test Problem 4

	$\vartheta = -10$		$\vartheta = 0$	
α	L_∞	κ	L_∞	κ
-10	2.6598e − 05	5.3441e + 08	3.8218e − 05	5.3696e + 08
-03	3.3559e − 05	5.3452e + 08	2.7566e − 05	5.3271e + 08
-02	3.5066e − 05	5.3504e + 08	2.5162e − 05	5.3221e + 08
00	3.8785e − 05	5.3660e + 08	2.8558e − 05	5.3133e + 08
02	4.3805e − 05	5.3893e + 08	6.8019e − 05	5.3597e + 08
03	4.7036e − 05	5.4041e + 08	3.9434e − 04	5.3866e + 08
10	2.2494e − 04	5.5670e + 08	2.9504e − 04	5.6261e + 08

Table 5. The numerical results generated using Haar wavelets for Test Problem 4

	$\vartheta = 2$		$\vartheta = 10$	
α	L_∞	κ	L_∞	κ
-10	4.3238e − 05	5.3938e + 08	2.2439e − 04	5.5741e + 08
-03	3.5767e − 05	5.3567e + 08	2.5779e − 04	5.5929e + 08
-02	3.4646e − 05	5.3548e + 08	2.5701e − 04	5.6030e + 08
00	6.7483e − 04	5.3623e + 08	2.7761e − 04	5.6309e + 08
02	2.5416e − 05	5.3965e + 08	7.5130e − 05	5.6705e + 08
03	8.5762e − 05	5.4213e + 08	8.7342e − 05	5.6948e + 08
10	8.4653e − 05	5.6667e + 08	4.4201e − 05	5.7578e + 08

Problem 5. *Consider the time-dependent problem in Equation (32), along with the functions:*

$$\begin{aligned} f(\varkappa,\mathfrak{y},\mathfrak{t}) &= -3(-\mathfrak{t}^2 + 2\varkappa + 2\mathfrak{y}),\\ \Re(\varkappa,\mathfrak{y}) &= \varkappa^3 + \mathfrak{y}^3,\\ \Im_1(\mathfrak{y},\mathfrak{t}) &= \mathfrak{y}^3 + \mathfrak{t}^3 - \alpha_1 \int_0^1 \alpha(\mathfrak{x})(\mathfrak{t}^3 + \mathfrak{y}^3 + \mathfrak{x}^3)d\mathfrak{x}\\ \Im_2(\mathfrak{y},\mathfrak{t}) &= 1 + \mathfrak{y}^3 + \mathfrak{t}^3 - \alpha_2 \int_0^1 \vartheta(\mathfrak{x})(\mathfrak{t}^3 + \mathfrak{y}^3 + \mathfrak{x}^3)d\mathfrak{x},\\ \Im_3(\varkappa,\mathfrak{t}) &= \varkappa^3 + \mathfrak{t}^3,\\ \Im_4(\varkappa,\mathfrak{t}) &= \varkappa^3 + 1 + \mathfrak{t}^3, \end{aligned} \tag{62}$$

where α_1 and α_2 are both set to 1. The exact solution is given by:

$$s(\varkappa,\mathfrak{y},\mathfrak{t}) = \varkappa^3 + \mathfrak{y}^3 + \mathfrak{t}^3. \tag{63}$$

We select ϑ values of -10, 0, 2, and 10, and set $d\mathfrak{t} = 0.0005$ with $T = 1$ to investigate how the accuracy of the proposed method depends on ϑ. The numerical results for different values of α (i.e., $\alpha = -10, -3, -2, 0, 2, 3, 10$) are presented in

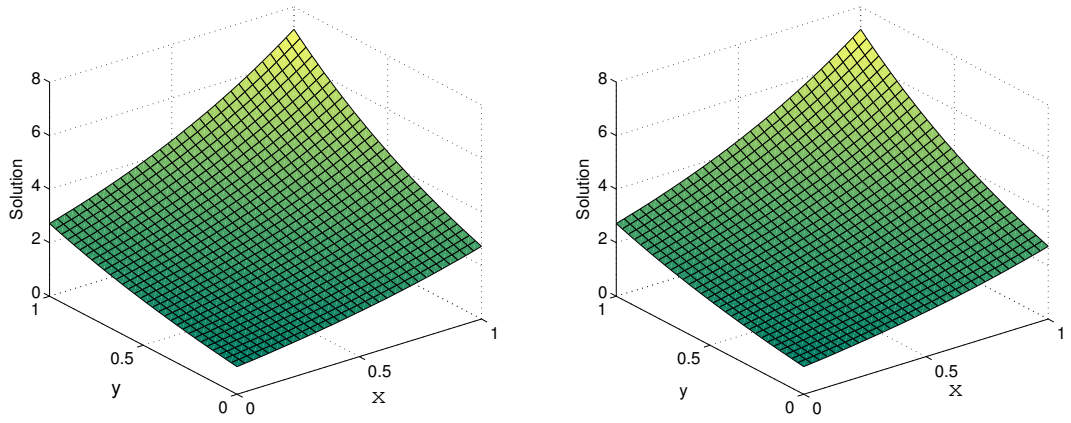

Figure 6. 3D view of results of Test Problem 4, exact (left) and numerical (right)

Tables 6 and 7.

Table 6. The numerical results generated using Haar wavelets for Test Problem 5 with $d\mathfrak{t} = 0.0005$ and $T = 1$

	$\vartheta = -10$		$\vartheta = 0$	
α	L_∞	κ	L_∞	κ
-10	$7.8361\text{e}-05$	$7.6785\text{e}+07$	$2.3985\text{e}-04$	$7.5307\text{e}+07$
-03	$2.3467\text{e}-04$	$7.8718\text{e}+07$	$8.2108\text{e}-05$	$4.7640\text{e}+07$
-02	$2.4293\text{e}-04$	$7.7328\text{e}+07$	$6.7607\text{e}-05$	$4.6673\text{e}+07$
00	$2.6320\text{e}-04$	$7.5864\text{e}+07$	$8.5138\text{e}-05$	$4.2737\text{e}+07$
02	$2.7061\text{e}-04$	$7.6323\text{e}+07$	$3.6215\text{e}-04$	$4.3677\text{e}+07$
03	$2.7821\text{e}-04$	$7.5311\text{e}+07$	$2.5000\text{e}-03$	$4.6090\text{e}+07$
10	$5.3735\text{e}-04$	$7.3153\text{e}+07$	$7.5906\text{e}+35$	$7.5623\text{e}+07$

Tables 6 and 7 display the error and condition number κ against various values of α and ϑ. All simulations used parameters T=1 and d$\mathfrak{t}$ =0.0005. The results indicate that, as expected, higher values of α lead to increased error variability in the non-deterministic case due to the propagation of rounding errors. For a fixed α, larger values of ϑ also result in inaccuracies due to the enhanced stiffness phenomenon.

Table 7. The numerical results generated using Haar wavelets for Test Problem 5 with $d\mathfrak{t} = 0.0005$ and $T = 1$

	$\vartheta = 2$		$\vartheta = 10$	
α	L_∞	κ	L_∞	κ
-50	$3.2004\text{e}-04$	$4.5696\text{e}+08$	$3.4810\text{e}-04$	$4.6848\text{e}+08$
-30	$2.7565\text{e}-04$	$2.6229\text{e}+08$	$3.5476\text{e}-04$	$3.3919\text{e}+08$
-10	$2.5726\text{e}-04$	$5.2507\text{e}+07$	$7.2413\text{e}-04$	$8.5954\text{e}+07$
-03	$2.1362\text{e}-04$	$4.7381\text{e}+07$	$3.3986\text{e}+13$	$7.7049\text{e}+07$
-02	$2.3705\text{e}-04$	$4.5438\text{e}+07$	$7.2951\text{e}+19$	$7.5279\text{e}+07$
00	$3.6899\text{e}-04$	$4.3639\text{e}+07$	$7.7906\text{e}+35$	$7.2383\text{e}+07$
02	$5.4200\text{e}-02$	$4.3476\text{e}+07$	$6.3430\text{e}+55$	$7.3907\text{e}+07$
03	$4.2767\text{e}+02$	$4.1867\text{e}+07$	$2.5365\text{e}+67$	$7.6128\text{e}+07$
10	$6.3430\text{e}+55$	$7.2669\text{e}+07$	$4.5071\text{e}+180$	$8.1231\text{e}+07$

It is important to note from Tables 6 and 7, that when $\vartheta = 0$ and $\alpha = 10$, the error escalates to an extremely large value of 7.5906×10^{35}, corresponding to a κ value of 7.5623×10^7. Moreover, for $\vartheta = 10$ and $\alpha = 10$ the error becomes significantly larger, reaching 4.5071×10^{180}, alongside a κ value of 8.1231×10^7. This suggests a complete failure of the simulation at these parameter values. Overall, the findings illustrate the impact of parameter choices on solution behavior, emphasizing the importance of selecting suitable values to ensure numerical stability and precision. Additional studies, such as evaluating the convergence of the method, could provide a deeper insight into the problem.

Figure 7 shows the numerical results of the proposed method in terms of the comparison between the L_∞ norm and the values of parameters α_1 and α_2, while Figure 8 compares the exact and numerical solutions.

5. Conclusions

The aim of the article is to numerically solve partial differential equations with integral boundary conditions using the Haar wavelets collocation method. It has investigated the method's efficacy and accuracy concerning nonlocal parameters α and ϑ. The numerical findings have indicated that the Haar wavelets approach has performed effectively and efficiently in addressing parabolic differential equations with integral boundary conditions, particularly when both α and ϑ have been negative. However, convergence has failed for the numerical methods when α and ϑ have exceeded 3. Maintaining α negative while keeping ϑ positive with equal magnitude or ensuring α magnitude has been greater than ϑ has enhanced accuracy. The collocation method has guaranteed that both the differential equation and integral boundary conditions have been met at designated

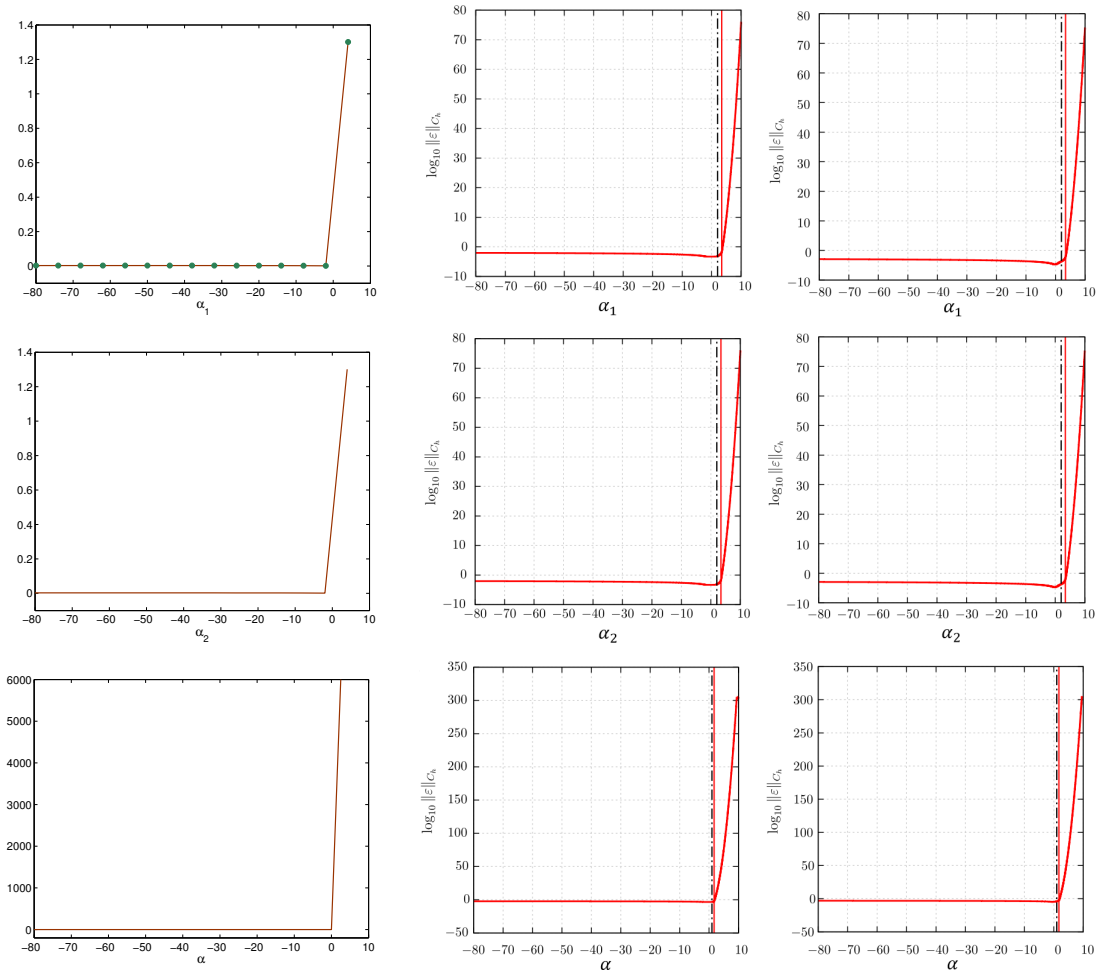

Figure 7. Comparison of the dependence of max-error on the values of parameters α_1 and α_2 with[42]: (1st row) $\alpha_1 = 0$, (2nd row) $\alpha_2 = 0$, (3rd row) $\alpha_1 = \alpha_2 = \alpha$, of Test Problem 5

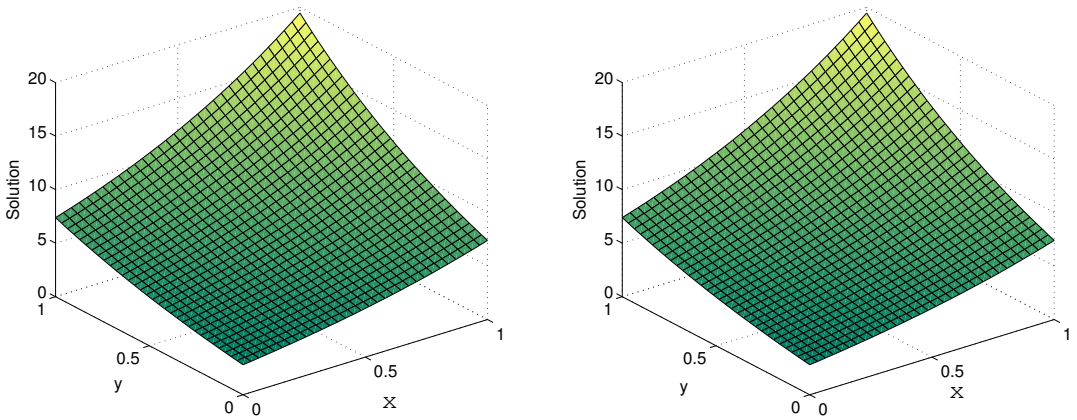

Figure 8. 3D view of results of Test Problem 5, exact (left) and numerical (right).

points, resulting in a set of algebraic equations that can be solved efficiently. The compact support and orthogonality of Haar wavelets have been particularly effective in managing non-smooth solutions and capturing steep gradients, making them well-suited for various parabolic problems involving integral boundary conditions. The Haar wavelet method maintains accuracy in the presence of noisy data or discontinuous coefficients, thanks to the localized support of Haar functions. However, when applied to irregular domains, the method would need to be extended using domain

decomposition or adaptive techniques. These enhancements are suggested as promising avenues for future research to broaden the method's applicability to real-world problems. Numerical tests have confirmed the method's effectiveness in terms of accuracy, integration, and computational efficiency, highlighting its practical applicability to real-world problems. The Haar wavelets collocation method has presented a promising approach for numerically treating PDEs with integral boundary conditions, providing a valuable tool for researchers and practitioners across various fields of science and engineering.

5.1. Future Work

This section outlines several avenues for extending current research. Specifically, we propose applying the Haar wavelet collocation method to two- and three-dimensional problems to assess its scalability and generality. Additionally, the use of adaptive Haar bases is recommended for handling complex or irregular domains more effectively. To enhance the method's robustness in practical scenarios, integrating noise-filtering techniques is also suggested. Finally, we recommend exploring hybrid approaches that combine Haar wavelets with other numerical schemes to improve flexibility and computational efficiency. These recommendations aim to guide future investigations and broaden the applicability of the proposed method.

Acknowledgments

None.

Funding

None.

Conflict of interest

The authors declare there is no competing interest regarding this work.

Author contributions

Conceptualization: Muhammad Nawaz Khan, Imtiaz Ahmad, Mohamed Mousa
Formal analysis: Muhammad Nawaz Khan, Masood Ahmad, Rashid Jan
Investigation: Mohamed Mousa, Rashid Jan, Imtiaz Ahmad
Methodology: Muhammad Nawaz Khan, Masood Ahmad, Mohamed Mousa
Writing-original draft: Muhammad Nawaz Khan, Imtiaz Ahmad
Writing-review & editing: Rashid Jan, Mohamed Mousa

Availability of data

Not applicable.

AI tools statement

All authors confirm that no AI tools were used in the preparation of this manuscript.

References

1. Bouziani A. On the solvability of parabolic and hyperbolic problems with a boundary integral condition. *Int J Math Math Sci.* 2002;31(4):201-213.
2. Barbu T, Miranville A, Moroşanu C. On a local and nonlocal second-order boundary value problem with in-homogeneous cauchy–neumann boundary conditions—applications in engineering and industry. *Mathematics.* 2024;12(13):2050.
3. Molaei H. Optimal control and problem with integral boundary conditions. *Int J Contemp Math Sci.* 2011;6(48):2385-2390.
4. Almomani R, Almefleh H. On heat conduction problem with integral boundary condition. *J Emerg Trends Eng Appl Sci.* 2012;3(6):977-979.
5. Bouziani A. On a class of parabolic equations with a nonlocal boundary condition. *Bulll'Acad R Belg.* 1999;10(1):61-77.
6. Yin H-M. On a class of parabolic equations with nonlocal boundary conditions. *J Math Anal Appl.* 2004;294(2):712-728.
7. Bouziani A. Strong solution for a mixed problem with nonlocal condition for certain pluriparabolic equations. *Hiroshima Math J.* 1997;27(3):373-390.
8. Day W. A decreasing property of solutions of parabolic equations with applications to thermoelasticity. *Qtly Appl Math.* 1983;40(4):468-475.
9. Ang W. A method of solution for the one-dimensional heat equation subject to nonlocal conditions. *Southeast Asian Bull Math.* 2003;26:185-191.
10. Dehghan M. Efficient techniques for the second-order parabolic equation subject to nonlocal specifications. *Appl Numer Math.* 2005;52(1):39-62.
11. Day W. Extensions of a property of the heat equation to linear thermoelasticity and other theories. *Qtly Appl Math.* 1982;40(3):319-330.
12. Kumar A, Kumar M, Goswami P. Numerical solution of coupled system of Emden–Fowler equations using artificial neural network technique. *Int J Optimiz Control Theor Appl.* 2024;14(1):62-73.
13. Arslan D, Çelik E. An approximate solution of singularly perturbed problem on uniform mesh. *Int J Optimiz Control Theor Appl.* 2024; **14**(1):74-80.

14. Baleanu D, Hajipour M, Jajarmi A. An accurate finite difference formula for the numerical solution of delay-dependent fractional optimal control problems. *Int J Optimiz Control Theor Appl.* 2024;14(3):183-192.
15. Abbas WS, El-wakad MT, Darwish RR. *Finite element modeling for two-dimensional wireless capsule endoscope manipulation system. Trends Adv Sci Technol.* 2025;2(1): 2.
16. Masti I, Sayevand K, Jafari H. On analyzing two-dimensional fractional order brain tumor model based on orthonormal Bernoulli polynomials and Newton's method. *Int J Optimiz Control Theor Appl.* 2024;14(1):12-19.
17. Malagi NS, Veeresha P, Prasanna GD, Prasannakumara BC, Prakasha DG. Novel approach for nonlinear time-fractional Sharma–Tasso–Olver equation using Elzaki transform. *Int J Optimiz Control Theor Appl.* 2023;13(1):46-58.
18. Erdogan U, Ozis T. A smart nonstandard finite difference scheme for second order nonlinear boundary value problems. *J Comput Phys.* 2011;230(17):6464-6474.
19. Mukhtarov O, ÇAVUŞOĞLU S, OLĞAR H. Numerical solution of one boundary value problem using finite difference method. *Turk J Math Comput Sci.* 2019;11:85-89.
20. Cheng F, Li W, Zhou Y, et al. admetSAR: a comprehensive source and free tool for assessment of chemical ADMET properties. *J Chem Inf Model.* 2012;52(11):3099-3105.
21. Hoppe RH, Kieweg M. Adaptive finite element methods for mixed control-state constrained optimal control problems for elliptic boundary value problems. *Comput Optimiz Appl.* 2010;46:511-533.
22. Hesameddini E, Riahi M. Hybrid legendre block-pulse functions method for solving partial differential equations with non-local integral boundary conditions. *J Inform Optimiz Sci.* 2019;40(7):1391-1403.
23. Siraj-ul-Isalm, Aziz I, Ahmad M. Numerical solution of two-dimensional elliptic PDEs with nonlocal boundary conditions. *Comput Math Appl.* 2015;69(3):180-205.
24. Ooi E H, Popov V. A simplified approach for imposing the boundary conditions in the local boundary integral equation method. *Comput Mech.* 2013;51(5):717-729.
25. Kai Y, Yin Z. On the gaussian traveling wave solution to a special kind of schrödinger equation with logarithmic nonlinearity. *Mod Phys Lett B.*, 2022;36(02):2150543.
26. Yang Y, Li H. Neural ordinary differential equations for robust parameter estimation in dynamic systems with physical priors. *Appl Soft Comput.* 2025;169:112649.
27. Chen Z, Wu J, Xu Y. Higher-order finite volume methods for elliptic boundary value problems. *Adv Comput Math.* 2012;37(2):191-253.
28. Jang G-W, Kim Y Y, Choi K K. Remesh-free shape optimization using the wavelet-Galerkin method. *Int J Solids Struct.* 2004;41(22-23):6465-6483.
29. Liu Y, Cen Z. Daubechies wavelet meshless method for 2-D elastic problems. *Tsinghua Sci Technol.* 2008;13(5):605-608.
30. Lepik Ü. Solving PDEs with the aid of two-dimensional haar wavelets. *Comput Math Appl.* 2011;61(7):1873-1879.
31. Díaz L A, Martín M T, Vampa V. Daubechies wavelet beam and plate finite elements. *Finite Elements Anal Des.* 2009;45(3):200-209.
32. Khan A A, Ahsan M, Ahmad I, Alwuthaynani M. Enhanced resolution in solving first-order nonlinear differential equations with integral condition: a high-order wavelet approach. *Eur Phys J Spec Top.* 2024;2024:1-14.
33. Ahsan M, Khan A A, Dinibutun S, et al. The haar wavelets based numerical solution of Reccati equation with integral boundary condition. *Thermal Sci.* 2023;27(1):93-100.
34. Shah K, Amin R, Abdeljawad T. Utilization of Haar wavelet collocation technique for fractal-fractional order problem. *Heliyon.* 2023;9(6):e17123.
35. Amin R, Shah K, Awais M, Mahariq I, Nisar KS, Sumelka W. Existence and solution of third-order integro-differential equations via Haar wavelet method. *Fractals* 2023;31(02):2340037.
36. Liu X, Ahsan M, Ahmad M, et al. Applications of haar wavelet-finite difference hybrid method and its convergence for hyperbolic nonlinear Schr ö dinger equation with energy and mass conversion. *Energies* 2021;14(23):7831.
37. Ahsan M, Lin S, Ahmad M, et al. A haar wavelet-based scheme for finding the control parameter in nonlinear inverse heat conduction equation. *Open Phys.* 2021;19(1): 722-734.
38. Zhou S, He Z, Chen X, Chang W. An anomaly detection method for uav based on wavelet decomposition and stacked denoising autoencoder. *Aerospace.* 2024;11(5):393.
39. Aziz I, Šarler B. The numerical solution of second-order boundary-value problems by collocation method with the haar wavelets. *Math Comput Model.* 2010;52(9-10):1577-1590.
40. Tatari M, Dehghan M. On the solution of the non-local parabolic partial differential equations via radial basis functions. *Appl Math Model.*, 2009;33(3):1729-1738.
41. Ivanauskas F, Meškauskas T, Sapagovas M. Stability of difference schemes for two-dimensional parabolic equations with non-local boundary conditions. *Appl Math Comput.* 2009;215(7):2716-2732.
42. Sajavičius S. Stability of the weighted splitting finite-difference scheme for a two-dimensional parabolic equation with two nonlocal integral conditions. *Comput Math Appl.* 2012;64(11):3485-3499.

Muhammad Nawaz Khan *earned his Ph.D. in Computational and Applied Mathematics from the University of Engineering and Technology (UET), Peshawar, Khyber Pakhtunkhwa, Pakistan, on April 2, 2022. His research focuses on the numerical and analytical study of mathematical models arising in applied sciences and engineering, with particular emphasis on computational techniques for solving differential equations. He has published 20 research articles in peer-reviewed journals, contributing significantly to the advancement of computational mathematics. Currently, he is working as a postdoctoral researcher at Institute of Engineering Mathematics, University Malaysia Perlis, Arau, Perlis, Malaysia.*
https://orcid.org/0000-0001-6447-6989

Masood Ahmad *earned his Ph.D. in Computational and Applied Mathematics from the University of Engineering and Technology (UET), Peshawar. His research focuses on global meshless methods using Radial Basis Functions (RBF) and Haar wavelets for solving interface problems and differential equations with simple, two-point, and integral boundary conditions. He has published 19 peer-reviewed articles, contributing to the advancement of meshless numerical methods in computational mathematics.*
https://orcid.org/0009-0001-3556-4450

Rashid Jan *holds both a Master's and an MPhil degree in mathematics from the University of Peshawar. In 2016, he was awarded a Chinese Government Scholarship to pursue his Ph.D. at Xi'an Jiaotong University, China, where he specialized in applied mathematics and completed his degree in June 2020. In 2021, he joined the Department of Mathematics at the University of Swabi as an Assistant Professor. He has published numerous research articles in high-impact journals. His editorial contributions include serving as a Guest Editor for various special issues and holding editorial positions with Frontiers and Scientific Reports. He also completed a 2-year postdoctoral research fellowship at Universiti Tenaga Nasional (UNITEN), Malaysia. In recognition of his scholarly output and academic influence, he was honored as a High-Ranked Scholar by ScholarGPS in 2024.*
https://orcid.org/0000-0001-9709-7045

Imtiaz Ahmad *holds a post-doctoral position at Universiti Tenaga Nasional (UNITEN) in Malaysia. He completed his Ph.D. in Computational Mathematics at the University of Engineering and Technology, Peshawar, Pakistan, in August 2017. His research focuses on the numerical solution of mathematical models in the form of ODEs, PDEs, and fractional PDEs, which arise in finance, computational biology, and various engineering disciplines. He has published more than 70 research articles in well-reputed ISI journals.*
https://orcid.org/0000-0002-4023-3293

Mohamed Moussa *joined the Faculty of Engineering and Technology in September 2006. He earned his Bachelor's degree in Electronics and Communications Engineering from the Faculty of Engineering and Technology at Future University in Egypt, graduating with distinction and a perfect cumulative GPA of 4.00. In September 2011, he was appointed as a Teaching Assistant in the Department of Electronics and Electrical Engineering (EED). In January 2012, he enrolled in the postgraduate program in Electronics and Communications Engineering at the Faculty of Engineering, Ain Shams University. He successfully completed 10 graduate-level courses with an outstanding cumulative GPA of 3.90. He completed his Ph.D. from Helwan University in 2022. He is an assistant Professor in Electrical Engineering Department-Future University In Egypt from 2022 till now.*
https://orcid.org/0000-0001-7290-7726

An International Journal of Optimization and Control: Theories & Applications
(https://accscience.com/journal/ijocta)